Available online at www.sciencedirect.com
SCIENCE DIRECT®
Journal of Sound and Vibration 272 (2004) 539–555
JOURNAL OF SOUND AND VIBRATION
www.elsevier.com/locate/jsvi

Hydroelastic vibration of two identical rectangular plates

Kyeong-Hoon Jeong[a,*], Gye-Hyoung Yoo[b], Seong-Cheol Lee[b]

[a] *Mechanical System Development Department, Korea Atomic Energy Research Institute, P.O. Box 105, Yusong, Daejeon 305–600, Republic of Korea*

[b] *Department of Mechanical Engineering, Chonbuk National University, Jeonju, Jeonbuk 560-756, Republic of Korea*

Received 27 August 2002; accepted 28 March 2003

Abstract

A theoretical study is presented on the hydroelastic vibration of two identical rectangular plates coupled with a bounded fluid. It is assumed that the plates are clamped along the plate edges and an ideal fluid is surrounded by the two rectangular plates and a rigid rectangular container. The velocity potential satisfying the fluid boundary conditions is expanded in terms of a finite Fourier series and the modal displacements of the plates are also expanded by the finite Fourier series for the compatibility requirement along the contacting surface between the plates and the fluid. Two transverse vibration modes, in-phase and out-of-phase, are observed in the symmetric fluid-coupled structure. Each in-phase mode is assumed as a combination of the beam modes in air, but every out-of-phase mode is assumed as a combination of polynomials satisfying the plate boundary condition and fluid volume conservation. The coupled natural frequencies are obtained from the relationship between the reference kinetic energy of the structure including the fluid and the maximum strain energy of the two plates. The proposed analytical method was found to be in good agreement with the results of a three-dimensional finite element analysis.

1. Introduction

It is generally known that the natural frequency of a structure in contact with a fluid, or immersed in a fluid, decreases significantly compared to the natural frequency of the corresponding dry mode. This problem is referred to as the fluid–structure interaction problem. For this problem, many investigators have suggested some approximate solutions which have been used to predict the changes in the natural frequencies of the structure in the fluid. In recent literature, there has been renewed interest in the problem of plates vibrating in contact with water. This is stimulated by new technical applications and also by the availability of powerful numerical

*Corresponding author. Tel.: +82-42-868-8792.
E-mail address: khjeong@kaeri.re.kr (K.-H. Jeong).

0022-460X/03/$ - see front matter © 2003 Elsevier Ltd. All rights reserved.
doi:10.1016/S0022-460X(03)00383-3

tools based on the finite element and boundary element methods that make numerical solutions of fluid–structure interaction problems possible. However, the use of the finite element method or the boundary element method requires enormous amounts of time for modelling and computation.

Rectangular plates vibrating in contact with fluid have recently been studied. Kim [1] derived an expression in terms of a series for the added virtual fluid mass of a simply supported rectangular plate which is chordwise finite and lengthwise semi-finite by using the Mathieu function. Kwak [2] studied the free vibrations of rectangular plates in contact with water on one side. In his numerical approach based on a piecewise division, beam functions were used as admissible functions, and the fluid was assumed to be unbounded. Fu and Price [3] studied the dry and wet dynamic characteristics of a vertical and horizontal cantilever plate by adopting a finite element discretization. Maylan [4] presented a forced vibration of an arbitrary thin plate floating on the surface of an infinite fluid using the Rayleigh–Ritz method. Muthuverrappan et al. also studied the free vibration of a cantilever square plate [5] and a cantilever rectangular plate [6] immersed in water, and they investigated the effect of the boundary conditions of the plate on the added mass of the fluid [7] using the finite element method. The finite element displacement method for a modal analysis of a plate in contact with fluid was developed by Hori et al. [8]. Haddara and Cao [9] studied the dynamic response of submerged rectangular plates. They derived an approximate expression of the modal added masses for cantilever rectangular plates and verified the theory by an experiment. Tayler and Ohkusu [10] suggest expressions for the free–free rectangular plates in terms of the sinusoidal eigenmodes of a pinned–pinned beam and rigid body modes. Asymptotic and numerical analyses of unsteady hydroelastic behavior of a floating plate due to given external loads were presented by Korobkin [11]. The main parameters in this paper were plate length and duration of the external loads. Liang et al. [12] suggested a simple procedure to determine the natural frequencies and mode shapes of submerged cantilever plates based on an empirical added mass formulation. Jeong [13] suggested an analytical method to calculate the coupled natural frequencies of two identical circular plates coupled with an ideal fluid, and verified the method by finite element analysis.

This paper describes a further application of the hydroelasticity theory [13] to the fluid–coupled rectangular plates, and deals with the coupling effect of contacting fluid on the free vibration characteristics of two identical rectangular plates supported by a rectangular rigid container filled with incompressible and frictionless fluid. Here it was assumed that the rectangular plates are clamped at their edges. The wet dynamic displacements of the plate are assumed to be the dry modal functions of a rectangular plate for the in-phase modes, and for the out-of-phase modes, they are assumed to be a polynomial function satisfying the boundary conditions and fluid volume conservation. The natural frequencies of both the in-phase modes and the out-of-phase modes can be obtained by theoretical calculations and finite element analyses for the fluid-coupled system.

2. Theoretical background

2.1. Formulation for rectangular plates

Fig. 1 represents two identical rectangular plates coupled with a fluid, where a, b and h represent the width, length and thickness of the rectangular plates, respectively. For the

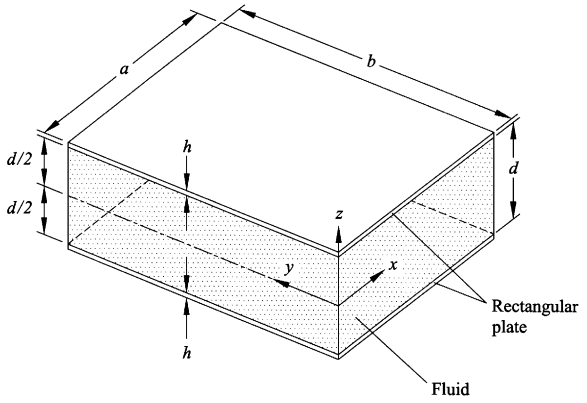

Fig. 1. Two identical rectangular plates coupled with bounded fluid.

theoretical formulation, the following assumptions are made: (a) the fluid motion is small; (b) the fluid is incompressible, inviscid and irrotational; (c) the gravity has an insignificant effect on the plate deflection curve; (d) the rectangular plates are made of linearly elastic, homogeneous, and isotropic material; and (e) the shear deformation and rotary inertia are negligible. The equation of motion for the transverse displacement, w_j, of these rectangular plates is

$$D\nabla^4 w_j + \rho h w_{j,tt} = P_j, \quad j = 1, 2, \tag{1}$$

and E is the Young's modulus of the plates. In this equation, $D = E\,h^3/12\,(1-\mu^2)$ is the flexural rigidity of the rectangular plates; $_\rho$, μ, and P_j are the plate density, the Poisson's ratio and hydrodynamic pressure on the rectangular plates, respectively. The upper rectangular plate is referred to with a subscript "1", while the lower one is denoted by a subscript "2." In addition,

$$\nabla^4 = \frac{\partial^4}{\partial x^4} + \frac{2\partial^4}{\partial y^2 \partial y^2} + \frac{\partial^4}{\partial y^4}, \tag{2}$$

is the bi-harmonic operator in the Cartesian co-ordinates x and y.

Using Rayleigh's quotients, we can obtain the frequency equations [5]

$$\omega_0^2 = (V_p/T_p^*)_{air}, \quad \omega_w^2 = \{V_p/(T_p^* + T_w^*)\}_{fluid}, \tag{3a, b}$$

where ω_0 is the natural frequency of the plate in air, ω_w is the fluid-coupled natural frequency, T_p^* and V_p are the reference kinetic energy and maximum strain energy, respectively, and T_w^* is the reference kinetic energy of the fluid due to the plate motion. It is necessary to find the appropriate mode shapes of the two plates in air and in contact with a fluid in order to calculate the kinetic and strain energies. However, it is very difficult to describe the wet mode shapes exactly in closed mathematical forms using Eq. (1). Therefore, each wet mode shape can be used as an appropriate admissible function W_{mn}, where m and n indicate the number of nodal lines with respect to the width and the length ($m = 0, 1, 2, \ldots$; $n = 0, 1, 2, \ldots$). The choice of an admissible function is very important to simplify the calcuations and to guarantee convergence to the actual solution. The

dynamic displacements, w_1 and w_2, can be assumed in the form of

$$w_1(x,y,t) = W_{mn}(x,y)\exp(\mathrm{i}\omega t) \quad \text{for the upper plate,} \tag{4a}$$

$$w_2(x,y,t) = q_{mn}W_{mn}(x,y)\exp(\mathrm{i}\omega t) \quad \text{for the lower plate,} \tag{4b}$$

where $\mathrm{i} = \sqrt{-1}$ and ω is the circular natural frequency of the plate. The admissible function, $W_{mn}(x,y)$ can be assumed as the eigenfunctions of the beams in air which satisfy the clamped boundary condition along the edges.

2.2. Natural frequency of a rectangular plate in air

When we consider the geometric boundary conditions along the edge of the plates, the slope and the displacement must be zero for the clamped boundary conditions, that is,

$$\left.\frac{\partial W_{mn}}{\partial x}\right|_{x=0} = W_{mn}|_{x=0} = \left.\frac{\partial W_{mn}}{\partial x}\right|_{x=a} = W_{mn}|_{x=a} = 0, \tag{5a}$$

$$\left.\frac{\partial W_{mn}}{\partial y}\right|_{y=0} = W_{mn}|_{y=0} = \left.\frac{\partial W_{mn}}{\partial y}\right|_{y=b} = W_{mn}|_{y=b} = 0. \tag{5b}$$

Therefore, the dynamic transverse displacement of the plates in air for the clamped edges can be assumed as a multiplication of clamped beam mode functions in air:

$$\begin{aligned} W_{mn}(x,y) = &\left[\cosh\left(\frac{\lambda_m x}{a}\right) - \cos\left(\frac{\lambda_m x}{a}\right) - \sigma_m\left\{\sinh\left(\frac{\lambda_m x}{a}\right) - \sin\left(\frac{\lambda_m x}{a}\right)\right\}\right] \\ &\times \left[\cosh\left(\frac{\lambda_n y}{b}\right) - \cos\left(\frac{\lambda_n y}{b}\right) - \sigma_n\left\{\sinh\left(\frac{\lambda_n y}{b}\right) - \sin\left(\frac{\lambda_n y}{b}\right)\right\}\right]. \end{aligned} \tag{6}$$

The coefficients, when $m = 1, 2, 3, \ldots$, $\lambda_m = 4.73004, 7.85320, 10.99561, 14.13717, 17.27876, (2m+1)\pi/2$ $(m > 4)$ and $\sigma_m = 0.98250, 1.00078, 0.99997, 1.00000$ $(m > 3)$; for n, the coefficients λ_n and σ_n are same. The trial function W_{mn}, is linearly independent, orthogonal and constitute a complete set.

The maximum potential energy of a rectangular plate can be computed with the admissible modal function

$$V_p = \frac{D}{2}\int_0^b \int_0^a \left(\left\{\frac{\partial^2 W_{mn}}{\partial x^2}\right\}^2 + \left\{\frac{\partial^2 W_{mn}}{\partial y^2}\right\}^2 + 2\mu\left\{\frac{\partial^2 W_{mn}}{\partial x^2}\right\}\left\{\frac{\partial^2 W_{mn}}{\partial y^2}\right\} + 2(1-\mu)\left\{\frac{\partial^2 W_{mn}}{\partial x\,\partial y}\right\}^2 \right) \mathrm{d}x\,\mathrm{d}y. \tag{7}$$

The maximum potential energy of the rectangular plate can be calculated by substitution of Eqs. (4) and (6) into Eq. (7) and integrating term by term. As the modal displacement is normalized, the reference kinetic energy of the plate is given as

$$T_p^* = \frac{1}{2}\rho h \int_0^b \int_0^a W_{mn}^2 \,\mathrm{d}x\,\mathrm{d}y = \frac{1}{2}\rho hab. \tag{8}$$

The natural frequency of the rectangular plate in air can be calculated by substituting the results of Eqs. (7) and (8) into Eq. (3a).

2.3. Velocity potential

First of all, the fluid motion must be defined in order to find the fluid-coupled natural frequencies and wet mode shapes of the two plates in contact with the fluid. Here we consider the fluid which is surrounded with the rectangular plates and rigid container walls. The three-dimensional oscillatory fluid flow can be described with the velocity potential. The facing side of the rectangular plates is contacted with a non-viscous and incompressible fluid. The fluid oscillation due to vibration of the plates can be described using the spatial velocity potential that satisfies the Laplace equation:

$$\nabla^2 \Phi(r, \theta, x, t) = 0. \tag{9}$$

It is possible to separate the function Φ with respect to x and y by observing that the container supporting the edges of the plates is assumed to be rigid, as in the case of the completely contacted rectangular plates. Thus, the general solution of Eq. (9) is

$$\Phi(x, y, z, t) = \mathrm{i}\omega\phi(x, y, z)\exp(\mathrm{i}\omega t). \tag{10}$$

When we consider the symmetry of the fluid velocities for the in-phase and out-of-phase vibration modes, the velocity potential will require the following symmetric conditions:

$$\frac{\partial\phi(x, y, -z)}{\partial z} = \frac{\partial\phi(x, y, z)}{\partial z} \quad \text{for the in-phase mode,} \tag{11a}$$

$$\frac{\partial\phi(x, y, z)}{\partial z} = 0 \quad \text{at } z = 0 \text{ for the out-of-phase mode.} \tag{11b}$$

Hence, the spatial velocity potential $\phi(x, y, z)$ satisfying Eq. (9) can be written as the following

$$\begin{aligned}\phi(x, y, z) = {} & \xi_{00} z + \sum_{r=1}^{\infty} \xi_{r0} \cos(\alpha_r x)\sinh(\alpha_r z) + \sum_{s=1}^{\infty} \xi_{0s} \cos(\beta_s y)\sinh(\beta_s z) \\ & + \sum_{r=1}^{\infty}\sum_{s=1}^{\infty} \xi_{rs} \cos(\alpha_r x)\cos(\beta_s y)\sinh(\gamma_{rs} z) \quad \text{for the in-phase modes,}\end{aligned} \tag{12a}$$

$$\begin{aligned}\phi(x, y, z) = {} & \xi_{00} z + \sum_{r=1}^{\infty} \xi_{r0} \cos(\alpha_r x)\cosh(\alpha_r z) + \sum_{s=1}^{\infty} \xi_{0s} \cos(\beta_s y)\cosh(\beta_s z) \\ & + \sum_{r=1}^{\infty}\sum_{s=1}^{\infty} \xi_{rs} \cos(\alpha_r x)\cos(\beta_s y)\cosh(\gamma_{rs} z) \quad \text{for the out-of-phase modes,}\end{aligned} \tag{12b}$$

where ξ_{00}, ξ_{r0}, ξ_{0s} and ξ_{rs} are the unknown coefficients which can be determined by the compatibility requirement of the fluid–structure interaction and

$$\alpha_r = r\pi/a, \quad \beta_s = s\pi/b, \quad \gamma_{rs} = \sqrt{\alpha_r^2 + \beta_s^2}. \tag{13a-c}$$

The boundary condition along the rigid container wall assures the zero fluid velocity, is given by

$$\left.\frac{\partial\phi}{\partial x}\right|_{x=0} = \left.\frac{\partial\phi}{\partial x}\right|_{x=a} = 0 \text{ at } x = 0 \text{ and } x = a \text{ of the rigid container wall,} \tag{14a}$$

$$\left.\frac{\partial\phi}{\partial y}\right|_{y=0} = \left.\frac{\partial\phi}{\partial y}\right|_{y=b} = 0 \text{ at } y = 0 \text{ and } y = b \text{ of the rigid container wall.} \tag{14b}$$

Eqs. (12a) and (12b) automatically satisfy the fluid boundary condition described by Eqs. (14a) and (14b).

2.4. Method of solution

In Eqs. (4a) and (4b), the coefficient q_{mn} can be determined by the symmetry of the modal displacements

$$q_{mn} = 1 \quad \text{for the in-phase modes,} \tag{15a}$$

$$q_{mn} = -1 \quad \text{for the out-of-phase modes.} \tag{15b}$$

The compatibility condition at the interface where the fluid contacts the plate surfaces is used to determine the unknown coefficients, ξ_{00}, ξ_{r0}, ξ_{0s} and ξ_{rs} of fluid motion in Eqs. (12a) and (12b). As the fluid displacement and the plate displacement must be equal in the transverse direction at the arbitrary interface surface between the fluid and the plate, the compatibility condition at the fluid interface with the plates yields

$$W_{mn} = \frac{\partial\phi}{\partial z} \quad \text{at } z = d/2, \tag{16a}$$

$$W_{mn} = \frac{\partial\phi}{\partial z} \quad \text{at } z = -d/2. \tag{16b}$$

Substitution of Eqs. (6), (12a) and (12b) into Eqs. (16a) and (16b) gives the following equations for the in-phase modes:

$$\begin{aligned}
&\left[\cosh\left(\frac{\lambda_m x}{a}\right) - \cos\left(\frac{\lambda_m x}{a}\right) - \sigma_m\left\{\sinh\left(\frac{\lambda_m x}{a}\right) - \sin\left(\frac{\lambda_m x}{a}\right)\right\}\right] \\
&\times\left[\cosh\left(\frac{\lambda_n y}{b}\right) - \cos\left(\frac{\lambda_n y}{b}\right) - \sigma_n\left\{\sinh\left(\frac{\lambda_n y}{b}\right) - \sin\left(\frac{\lambda_n y}{b}\right)\right\}\right] \\
&\quad = \xi_{00} + \sum_{r=1}^{\infty}\xi_{r0}\alpha_r \cos(\alpha_r x)\cosh(\alpha_r d/2) + \sum_{s=1}^{\infty}\xi_{0s}\beta_s\cos(\beta_s y)\cosh(\beta_s d/2) \\
&\qquad + \sum_{r=1}^{\infty}\sum_{s=1}^{\infty}\xi_{rs}\gamma_{rs}\cos(\alpha_r x)\cos(\beta_s y)\cosh(\gamma_{rs} d/2),
\end{aligned} \tag{17a}$$

and for the out-of-phase modes:

$$\left[\cosh\left(\frac{\lambda_m x}{a}\right)-\cos\left(\frac{\lambda_m x}{a}\right)-\sigma_m\left\{\sinh\left(\frac{\lambda_m x}{a}\right)-\sin\left(\frac{\lambda_m x}{a}\right)\right\}\right]$$
$$\times\left[\cosh\left(\frac{\lambda_n y}{b}\right)-\cos\left(\frac{\lambda_n y}{b}\right)-\sigma_n\left\{\sinh\left(\frac{\lambda_n y}{b}\right)-\sin\left(\frac{\lambda_n y}{b}\right)\right\}\right]$$
$$=\xi_{00}+\sum_{r=1}^{\infty}\xi_{r0}\alpha_r\cos(\alpha_r x)\sinh(\alpha_r d/2)+\sum_{s=1}^{\infty}\xi_{0s}\beta_s\cos(\beta_s y)\sinh(\beta_s d/2)$$
$$+\sum_{r=1}^{\infty}\sum_{s=1}^{\infty}\xi_{rs}\gamma_{rs}\cos(\alpha_r x)\cos(\beta_s y)\sinh(\gamma_{rs}d/2). \tag{17b}$$

Expanding the sinusoidal functions and hyperbolic functions in the left side of Eqs. (17a) and (17b) into a finite Fourier series gives

$$\cosh(\lambda_m x/a)=a_{m0}+\sum_{r=1}^{\infty}a_{mr}\cos(\alpha_r x),\quad \cos(\lambda_m x/a)=b_{m0}+\sum_{r=1}^{\infty}b_{mr}\cos(\alpha_r x),$$
$$\sinh(\lambda_m x/a)=c_{m0}+\sum_{r=1}^{\infty}c_{mr}\cos(\alpha_r x),\quad \sin(\lambda_m x/a)=g_{m0}+\sum_{r=1}^{\infty}g_{mr}\cos(\alpha_r x), \tag{18a–d}$$

with

$$a_{m0}=\sinh(\lambda_m)/\lambda_m,\quad b_{m0}=\sin(\lambda_m)/\lambda_m,$$
$$c_{m0}=\{\cosh(\lambda_m)-1\}/\lambda_m,\quad g_{m0}=\{1-\cos(\lambda_m)\}/\lambda_m, \tag{19a–d}$$

$$a_{mr}=\frac{2\lambda_m\sinh(\lambda_m)(-1)^r}{(\pi r)^2+\lambda_m^2},\quad b_{mr}=\frac{\sin(\pi r-\lambda_m)}{\pi r-\lambda_m}+\frac{\sin(\pi r+\lambda_m)}{\pi r+\lambda_m},$$
$$c_{mr}=\frac{2\lambda_m\{\cosh(\lambda_m)(-1)^r-1\}}{(\pi r)^2+\lambda_m^2},\quad g_{mr}=\left[\frac{\cos(\pi r-\lambda_m)-1}{\pi r-\lambda_m}\right]-\left[\frac{\cos(\pi r+\lambda_m)-1}{\pi r+\lambda_m}\right]. \tag{20a–d}$$

Similarly, the Fourier coefficients in the y direction can also be defined. The finite Fourier series expansion of the modal displacement shown in Eq. (6) gives

$$W_{mn}(x,y)=\Lambda_{00}+\sum_{r=1}^{\infty}\Lambda_{mr0}\cos(\alpha_r x)+\sum_{s=1}^{\infty}\Lambda_{n0s}\cos(\beta_s y)+\sum_{r=1}^{\infty}\sum_{s=1}^{\infty}\Lambda_{mnrs}\cos(\alpha_r x)\cos(\beta_s y). \tag{21}$$

Therefore, the velocity potential of the fluid can be written explicitly by arranging Eqs. (17a) and (17b), (18a–d) and (21). In Eqs. (18)–(21), the sum on r and s must be stopped for numerical computation, at an integer value large enough to give the required accuracy.

Now, it is necessary to know the reference kinetic energies of the plates and the contained fluid to calculate the coupled natural frequencies of the rectangular plates in contact with the fluid. Using the hypothesis of irrotational movement of the fluid, the reference kinetic energy of the fluid

can be evaluated from its boundary motion

$$T_F^* = \tfrac{1}{2}\rho_0 \int_0^a \int_0^b (\partial\phi(x,y,z)/\partial z)_{z=d/2}\, \phi(x,y,d/2)\,\mathrm{d}x\,\mathrm{d}y + \tfrac{1}{2}\rho_0 \int_0^a \int_0^b (\partial\phi(x,y,z)/\partial z)_{z=-d/2}\, \phi(x,y,-d/2)\,\mathrm{d}x\,\mathrm{d}y, \tag{22}$$

where ρ_0 is the mass density of fluid. Application of Eqs. (16a) and (16b) into Eq. (22) reduces to

$$T_F^* = -\tfrac{1}{2}\rho_0 \left(\int_0^b \int_0^a W_{mn}\phi(x,y,d/2)\,\mathrm{d}x\,\mathrm{d}y + \int_0^b \int_0^a W_{mn}\phi(x,y,-d/2)\,\mathrm{d}x\,\mathrm{d}y \right). \tag{23}$$

The reference kinetic energy of the two rectangular plates will be twice the value given in Eq. (8). That is

$$T_p^* = \rho\, h\, a\, b. \tag{24}$$

The maximum potential energy of the two plates also can be computed as twice of the kinetic energies of the eigenfunctions in Eq. (7). The fluid-coupled natural frequencies can be obtained by using Eq. (3b) which shows a relationship between the reference kinetic energies and the maximum potential energy.

2.5. Improved solution for out-of-phase modes

Instead of the dry beam functions of Eq. (6), normalized polynomial functions are introduced for the out-of-phase wet modes, because several beam functions of Eq. (6) cannot satisfy the fluid-volume conservation. The normalized polynomial functions are also the admissible functions satisfying all the plate boundary conditions of Eqs. (5a) and (5b) and fluid-volume conservation of Eq (26). The admissible functions are plotted in Fig. 2:

$$\begin{aligned}
X_0(x) &= \frac{1}{A_0}\left[\left(\frac{x}{a}\right)^2 - 2\left(\frac{x}{a}\right)^3 + \left(\frac{x}{a}\right)^4\right] = \frac{Q_0(x)}{A_0},\\
X_1(x) &= \frac{1}{A_1}\left[\frac{1}{2}\left(\frac{x}{a}\right)^2 - 2\left(\frac{x}{a}\right)^3 + \frac{5}{2}\left(\frac{x}{a}\right)^4 - \left(\frac{x}{a}\right)^5\right] = \frac{Q_1}{A_1},\\
X_2(x) &= \frac{1}{A_2}\left[\frac{3}{14}\left(\frac{x}{a}\right)^2 - \frac{10}{7}\left(\frac{x}{a}\right)^3 + \frac{45}{14}\left(\frac{x}{a}\right)^4 - 3\left(\frac{x}{a}\right)^5 + \left(\frac{x}{a}\right)^6\right] = \frac{Q_2}{A_2},\\
X_3(x) &= \frac{1}{A_3}\left[-\frac{3}{32}\left(\frac{x}{a}\right)^2 + \frac{7}{8}\left(\frac{x}{a}\right)^3 - \frac{95}{32}\left(\frac{x}{a}\right)^4 + \frac{75}{16}\left(\frac{x}{a}\right)^5 - \frac{7}{2}\left(\frac{x}{a}\right)^6 + \left(\frac{x}{a}\right)^7\right] = \frac{Q_3}{A_3},
\end{aligned} \tag{25a–d}$$

$$\int_0^a X_k(x)\,\mathrm{d}x = 0, \quad k = 0,1,2,3,\ldots, \tag{26}$$

where $A_k (k = 0,1,2,3,\ldots)$ is a factor for the mode normalization

$$A_k = \sqrt{\int_0^a \{Q_k(x)\}^2\,\mathrm{d}x}. \tag{27}$$

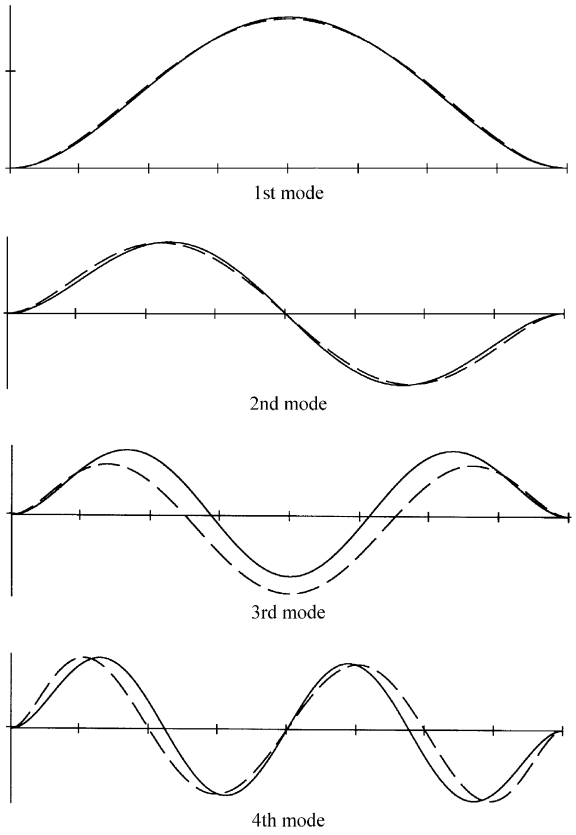

Fig. 2. Comparison of approximated modal functions (—— beam modal function, – – – polynomial approximation).

The polynomial functions $Y_k(y)$ ($k = 0, 1, 2, 3\ldots$) in the y direction also can be similarily defined. However, the first modal function $X_0(x)$ need not satisfy Eq. (25) because the other modal function $Y_k(y)$ will compensate the fluid-volume conservation in the y direction. The transverse modal function for the out-of-phase wet modes can be defined by a multiplication of x and y directional polynomial functions:

$$W_{mn}(x, y) = X_m(x)\, Y_n(y). \tag{28}$$

The modal functions approximated by Eqs. (25a–d) and (28) can also be expressed in terms of a Fourier series expansion using the finite Fourier transformation as described in

$$\left(\frac{x}{a}\right)^2 = \frac{1}{3} + 4\sum_{m=1}^{\infty} \frac{(-1)^m}{(m\pi)^2} \cos\left(\frac{m\pi x}{a}\right),$$

$$\left(\frac{x}{a}\right)^3 = \frac{1}{4} + 6\sum_{m=1}^{\infty} \left[\frac{2[1-(-1)^m]}{(m\pi)^4} + \frac{(-1)^m}{(m\pi)^2}\right] \cos\left(\frac{m\pi x}{a}\right),$$

$$\left(\frac{x}{a}\right)^4 = \frac{1}{5} + 8\sum_{m=1}^{\infty} \frac{[-6+(m\pi)^2](-1)^m}{(m\pi)^4} \cos\left(\frac{m\pi x}{a}\right),$$

$$\left(\frac{x}{a}\right)^5 = \frac{1}{6} + 10\sum_{m=1}^{\infty}\left[\frac{24\{(-1)^m - 1\}}{(m\pi)^6} + \frac{\{(m\pi)^2 - 12\}(-1)^m}{(m\pi)^4}\right]\cos\left(\frac{m\pi x}{a}\right),$$

$$\left(\frac{x}{a}\right)^6 = \frac{1}{7} + 12\sum_{m=1}^{\infty}\frac{[120 - 20(m\pi)^2 + (m\pi)^4](-1)^m}{(m\pi)^6}\cos\left(\frac{m\pi x}{a}\right),$$

$$\left(\frac{x}{a}\right)^7 = \frac{1}{8} + 14\sum_{m=1}^{\infty}\left[\frac{720\{1 - (-1)^m\}}{(m\pi)^8} + \frac{\{360 - 30(m\pi)^2 + (m\pi)^4\}(-1)^m}{(m\pi)^6}\right]\cos\left(\frac{m\pi x}{a}\right). \quad (29a-f)$$

The admissible functions of Eqs. (25a–d) and (28) can be transformed into Eq. (21) by using Eqs. (29a–f). Using the compatibility condition of Eqs. (16a) and (16b), relationships between the coefficients, Λ_{00}, Λ_{mr0}, Λ_{n0s}, Λ_{mrs} and ξ_{00}, ξ_{r0}, ξ_{0s}, ξ_{rs} can be obtained. The maximum potential energy of the two plates can be computed using the assumed polynomial functions of Eqs. (25a–d) and $Y_k(y)$ and the reference kinetic energy of the fluid can be obtained by Eqs. (22) and (28). For this case, the fluid-coupled natural frequencies can easily be calculated according to the same process in Section 2.4.

3. Example and discussion

3.1. An example model for theoretical calculation and finite element analysis

On the basis of the preceding analysis, in order to find the natural frequencies of two identical rectangular plates in air or coupled with the bounded fluid by the rigid container wall, Eqs. (3a) and (3b) is calculated using the commercially available software, Mathcad (version 2000 Professional) [14]. The frequency equation derived in the preceding sections involves an infinite series of algebraic terms. In the theoretical calculation, the finite Fourier expansion terms r and s are set at 900, which give a converged solution.

In order to check the validity of the theory, a finite element analysis was carried out for the bounded fluid-coupled system using ANSYS, release 5.7 finite element software [15]. A finite element model is constructed with the same plate geometry, boundary conditions and material properties used in the theoretical calculation. The plates are made of aluminum having an area of 240 mm × 320 mm and a thickness of 2 mm. The distance between the rectangular plates, d, is 40 mm. The physical properties of the material are as follows: Young's modulus = 69.0 GPa, the Poisson ratio = 0.3, and mass density = 2700 kg/m^3. Water is used as the fluid in contact with the plates, having a density of 1000 kg/m^3. The viscosity and compressibility of water are neglected in both the theoretical calculation and the finite element analysis.

The finite element analysis was performed to obtain the natural frequencies and mode shapes of the two identical rectangular plates coupled with bounded fluid. Here the three-dimensional model consisted of three-dimensional contained fluid elements (FLUID80) and elastic shell elements (SHELL63). The fluid element 'FLUID80' with eight nodes has three degrees of freedom at each node and it is particularly well suited for calculating hydrostatic pressures and fluid–structure interactions. The shell element 'SHELL63' with four nodes has six degrees of freedom: translation in three directions and rotations about three axes. The fluid movement along the rigid

walls is restricted to the normal direction only in order to realize Eqs. (14a) and (14b). The vertical velocity of the fluid element nodes adjacent to each surface of the wetted rectangular plates coincides to those of the rectangular plates so that the finite element model can simulate Eqs. (16a) and (16b). Each rectangular plate is identically meshed and divided into 1200 (40×30) elastic shell elements and the fluid region consists of 6000 ($40 \times 30 \times 5$) fluid elements with connectivity to the plate elements. A clamped boundary condition along each plate edge is applied in the finite element model to constrain against displacements and rotations. The finite element analysis used a block Lanczos method to extract 50 modal frequencies and corresponding mode shapes.

3.2. Comparison of theoretical and finite element results

The theoretical natural frequencies of the rectangular plate in air are listed and compared with the FEM results in Table 1. The discrepancy between the theoretical and FEM results is less than 0.7% in the range of $0 \leqslant n \leqslant 3$ and $0 \leqslant m \leqslant 3$. It shows that the combination of the beam modes can approximate the plate mode shapes excellently for the rectangular plate in air with the clamped boundary condition.

All the transverse vibration modes can be classified into two categories according to the relative moving directions between the two plates during vibration; that is, in-phase and out-of-phase modes. The fluid-coupled natural frequencies of the plates with $d = 40$ mm for the out-of-phase and in-phase modes are listed in Tables 2 and 3, respectively, in the range of $0 \leqslant n \leqslant 3$ and

Table 1
Comparison of FEM and theoretical natural frequencies (Hz) for a clamped rectangular plate in air

Mode		Natural frequency (Hz)		
n	m	FEM	Theory	Discrepancy (%)
0	0	242.6	243.4	0.33
	1	407.5	409.1	0.52
	2	677.6	681.3	0.55
	3	1047.3	1053.0	0.54
1	0	570.8	573.3	0.44
	1	722.3	726.9	0.64
	2	978.2	984.2	0.61
	3	1336.5	1345.5	0.67
2	0	1069.9	1074.2	0.40
	1	1216.0	1223.5	0.62
	2	1462.5	1470.3	0.53
	3	1810.6	1820.0	0.52
3	0	1736.3	1742.4	0.35
	1	1879.9	1891.1	0.60
	2	2121.3	2133.0	0.55
	3	2463.1	2474.9	0.48

Table 2
FEM and theoretical natural frequencies (Hz) of two identical rectangular plates coupled with fluid for the out-of-phase modes

Mode		Coupled natural frequency (Hz)				
n	m		Beam mode approximation		Polynomial approximation	
		FEM	Theory	Discrepancy (%)	Theory	Discrepancy (%)
0	0	N/A	N/A	N/A	N/A	N/A
	1	58.6	61.2	4.44	59.4	1.36
	2	155.0	194.6	25.55	159.4	2.84
	3	310.1	249.4	−19.57	287.2	−7.38
1	0	104.0	108.4	4.23	106.6	2.50
	1	167.6	176.6	5.37	170.1	1.49
	2	286.2	278.5	−2.69	281.3	−1.71
	3	463.2	447.6	−3.37	465.9	0.58
2	0	301.7	356.1	18.03	307.8	2.02
	1	389.2	322.7	−17.09	381.9	−1.88
	2	510.7	542.9	6.31	494.5	−3.17
	3	719.3	654.9	−8.95	710.5	−1.22
3	0	625.0	511.3	−18.19	593.4	−5.06
	1	722.9	660.9	−8.58	725.6	0.37
	2	883.3	825.9	−6.50	890.7	−0.84
	3	1106.9	1060.8	−4.16	1122.5	1.41

$0 \leqslant m \leqslant 3$. It was found that the theoretical natural frequencies of the in-phase mode agree well, within a 3% error range, with the finite element predictions as shown in Table 3 indicating that the dry beam functions can accurately approximate the in-phase modes. As shown in Table 3, the dry beam mode approximation underestimates the fluid virtual added mass with the error increasing with the mode number. On the other hand, the maximum deviation of the theoretical natural frequency from the finite element result for the out-of-phase modes is about 25% in the same mode range. This shows that the approximation based on the dry beam functions is inappropriate for the out-of-phase modes, because the dry beam functions cannot satisfy the fluid-volume conservation for several modes, for example, $n = 2$ or $m = 2$. However, as the number of modes in the dry beam mode approximation method increases, the discrepancy reduces gradually because the difference between the real mode shape and approximated admissible function decreases.

The polynomial functions of Eqs. (25a–d) satisfying the plate boundary conditions and fluid-volume conservation give more accurate results for the out-of-phase modes as shown in Table 2. Figs. 3 and 4 obtained from the finite element analysis illustrate a comparison between the in-phase and out-of-phase mode shapes. There is little difference between the in-phase mode shapes and the corresponding dry mode shapes because the in-phase modes are free from the fluid-volume conservation requirement. Hence we can get excellent theoretical result for the in-phase modes by the dry beam mode approximation. On the other hand, for the out-of-phase modes,

Table 3
FEM and theoretical natural frequencies (Hz) for two identical rectangular plates coupled with fluid for the in-phase modes

Mode		Coupled natural frequency (Hz)		
n	m		Beam mode approximation	
		FEM	Theory	Discrepancy(%)
0	0	113.3	114.1	0.71
	1	192.5	194.5	1.04
	2	326.5	330.9	1.35
	3	516.1	524.7	1.67
1	0	272.4	275.4	1.10
	1	348.4	353.9	1.58
	2	479.6	488.5	1.86
	3	668.8	683.8	2.24
2	0	525.9	533.3	1.41
	1	603.0	614.7	1.94
	2	735.4	751.4	2.18
	3	926.7	949.9	2.50
3	0	882.8	898.4	1.77
	1	962.8	985.1	2.32
	2	1099.0	1127.6	2.60
	3	1294.5	1332.5	2.94

some distorted mode shapes can be found in Fig. 4, because the plate must be deformed to satisfy the fluid-volume conservation requirement. This is especially the case for the 10th serial mode (510.7 Hz) which is the most distorted mode from the dry mode and corresponds to the $(m, n) = (2, 2)$ mode consisting of a combination of the special modal function similar to the third polynomial function in Fig. 2.

The coupled natural frequency of the two plates in contact with fluid is always less than the corresponding natural frequency of the plate in air, due to a contribution of the virtual added mass to the motion of the plates. Hence, the normalized natural frequency, defined as the natural frequency of a structure in contact with a fluid divided by the corresponding natural frequency of the structure in air, always lies between unity and zero as shown in Table 4.

The out-of-phase mode with $n = 0$ and $m = 0$ cannot appear because this mode violates the fluid-volume conservation for the bounded-fluid case. The first fluid-coupled natural frequency ($n = 0$, $m = 1$) for the out-of-phase mode is reduced to about 24% of the dry mode natural frequency. For the corresponding in-phase mode, however, the natural frequency has been reduced to about 34% of the dry mode value. It was observed that most of the normalized natural frequency decreases with an increase of mode number m, but increases with an increase of the mode n.

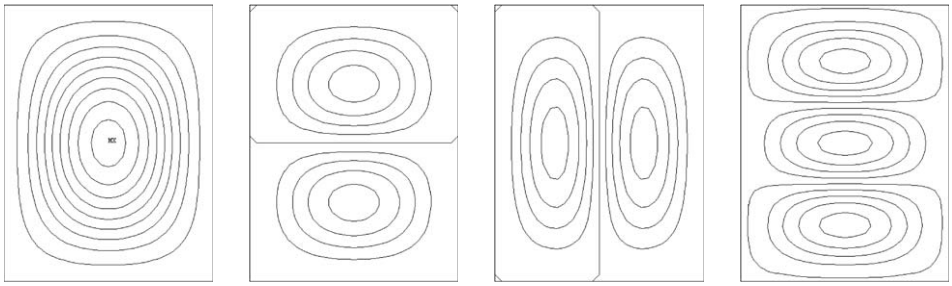

1st (113.3 Hz) 2nd (192.5 Hz) 3rd (272.4 Hz) 4th (326.5 Hz)

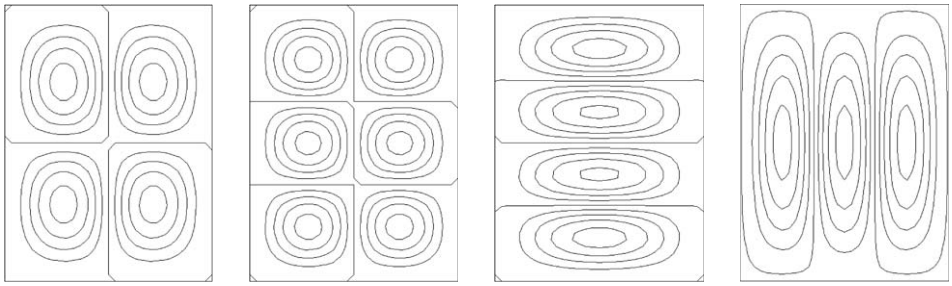

5th (348.4 Hz) 6th (479.6 Hz) 7th (516.1 Hz) 8th (525.9 Hz)

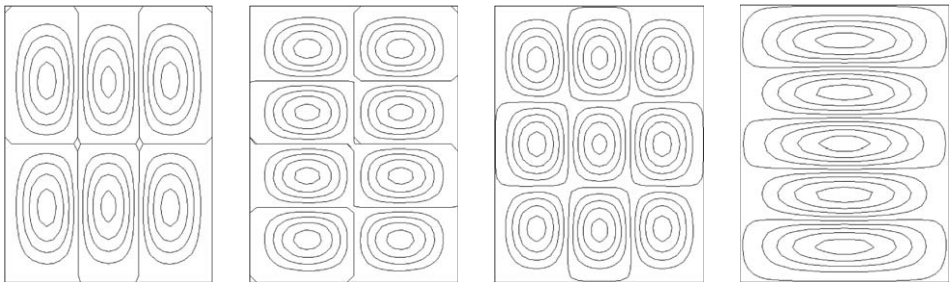

9th (603.0 Hz) 10th (668.8 Hz) 11th (735.4 Hz) 12th(764.8 Hz)

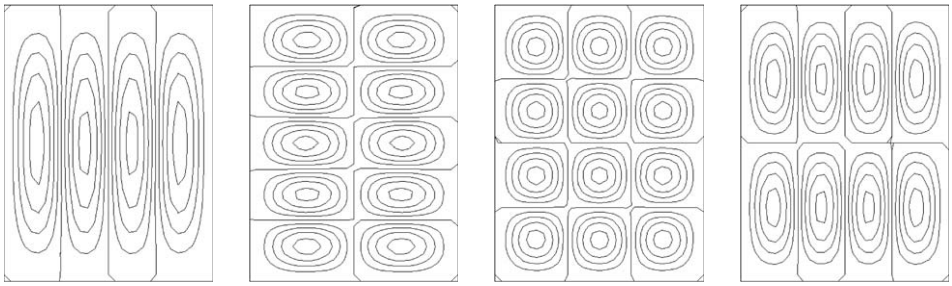

13th (882.8 Hz) 14th (918.8 Hz) 15th (926.7 Hz) 16 th(962.8 Hz)

Fig. 3. In-phase mode shapes for two rectangular plates coupled with fluid (FEM results).

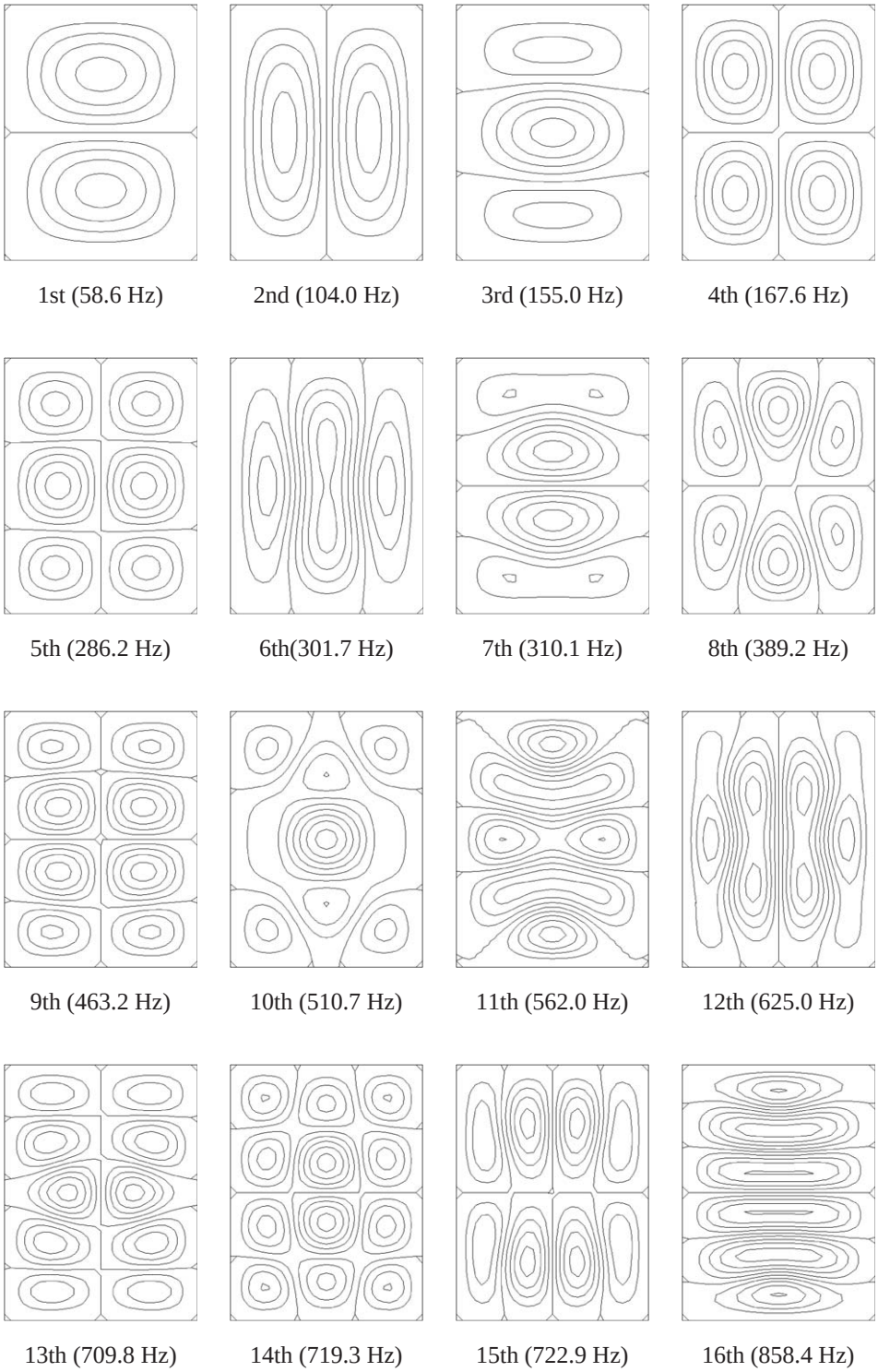

Fig. 4. Out-of-phase mode shapes for two rectangular plates coupled with fluid (FEM results).

Table 4
Normalized natural frequencies for two identical rectangular plates coupled with the fluid

Mode		Normalized natural frequency	
n	*m*	In-phase modes	Out-of-phase modes
0	0	0.4670	N/A
	1	0.3372	0.2415
	2	0.3052	0.2715
	3	0.2972	0.1786
1	0	0.6693	0.2555
	1	0.4823	0.2320
	2	0.3944	0.2354
	3	0.3558	0.2464
2	0	0.7761	0.4452
	1	0.6164	0.3979
	2	0.5028	0.3492
	3	0.4369	0.3391
3	0	0.8429	0.5968
	1	0.7204	0.5409
	2	0.6070	0.4878
	3	0.5256	0.4494

4. Conclusions

An analytical method to estimate the natural frequencies of two identical rectangular plates coupled with an ideal fluid is developed by using a finite Fourier series expansion method. It has been shown that there are two contrastive modes: the so-called out-of-phase and in-phase modes. All natural frequencies of the in-phase modes can be predicted well by the dry beam modes, but the natural frequency of the out-of-phase mode cannot be estimated precisely. However, the theoretical prediction for the out-of-phase mode can be improved by using the polynomials satisfying the plate boundary condition and fluid-volume conservation. The accuracy of the proposed analytical method has been verified by good agreement with results of a detailed three-dimensional finite element analysis.

References

[1] K.C. Kim, J.S. Kim, The effect of the boundary condition on the added mass of a rectangular plate, *Journal of the Society of Naval Architects of Korea* 15 (1978) 1–11 (in Korean).
[2] M.K. Kwak, Hydroelastic vibration of rectangular plates, *Transactions of the American Society of Mechanical Engineers, Journal of Applied Mechanics* 63 (1996) 110–115.
[3] Y. Fu, W.G. Price, Interactions between a partially or totally immersed vibrating cantilever plate and the surrounding fluid, *Journal of Sound and Vibration* 118 (1987) 495–513.

[4] M.H. Maylan, The forced vibration of a thin plate floating on an infinite liquid, *Journal of Sound and Vibration* 205 (1997) 581–591.
[5] G. Muthuveerappan, N. Ganesan, M.A. Veluswami, Vibration of square cantilever plate immersed in water, *Journal of Sound and Vibration* 61 (1978) 467–470.
[6] G. Muthuveerappan, N. Ganesan, M.A. Veluswami, A note on vibration of a cantilever plate immersed in water, *Journal of Sound and Vibration* 63 (1979) 435–460.
[7] G. Muthuveerappan, N. Ganesan, M.A. Veluswami, Influence of fluid added mass on the vibration characteristics of plates under various boundary conditions, *Journal of Sound and Vibration* 69 (1980) 612–615.
[8] Y. Hori, M. Kanoi, F. Fujisawa, Two dimensional coupling vibration analysis of fluid and structure using FEM displacement method, *Transactions of the Japan Society of Mechanical Engineers (Division C)* 60 (1994) 12–17 (in Japanese).
[9] M.R. Haddara, S. Cao, A study of the dynamic response of submerged rectangular flat plates, *Marine Structures* 9 (1996) 913–933.
[10] R.E. Tayler, M. Ohkusu, Green functions for hydroelastic analysis of vibrating free–free beams and plates, *Applied Ocean Research* 22 (2000) 295–314.
[11] A. Korobkin, Unsteady hydro-elasticity of floating plates, *Journal of Fluids and Structures* 14 (2000) 971–991.
[12] C.C. Liang, C.C. Liao, Y.S. Tai, W.H. Lai, The free vibration analysis of submerged cantilever plates, *Ocean Engineering* 28 (2001) 1225–1245.
[13] K.H. Jeong, Free vibration of two identical circular plates coupled with bounded fluid, *Journal of Sound and Vibration* 260 (2003) 653–670.
[14] Mathcad User's Guide—Mathcad 2000 Professional, MathSoft, Inc., Cambridge, MA, 1999.
[15] P. Kohnke, ANSYS theory reference, ANSYS elements reference, ANSYS command reference, release 5.4, SAS IP, Inc., 1997.